Available online at www.sciencedirect.com
SCIENCE DIRECT
Journal of Solid State Chemistry 179 (2006) 2595–2601
JOURNAL OF SOLID STATE CHEMISTRY
www.elsevier.com/locate/jssc

Crystal structures and magnetic properties of 6H-perovskite-type oxides $Ba_3MIr_2O_9$ (M = Mg, Ca, Sc, Ti, Zn, Sr, Zr, Cd and In)

Takeshi Sakamoto, Yoshihiro Doi*, Yukio Hinatsu

Division of Chemistry, Graduate School of Science, Hokkaido University, Sapporo 060-0810, Japan

Received 17 November 2005; received in revised form 13 March 2006; accepted 8 April 2006
Available online 19 May 2006

Abstract

Crystal structures and magnetic properties of quaternary oxides $Ba_3MIr_2O_9$ (M = Mg, Ca, Sc, Ti, Zn, Sr, Zr, Cd and In) were investigated. Rietveld analyses of their X-ray diffraction data indicate that they adopt the 6H-perovskite-type structure with space group $P6_3/mmc$ or, in the case of M = Ca, Sr and Cd, a monoclinically distorted structure with space group $C2/c$. The Ir valence configurations are $Ba_3M^{2+}Ir_2^{5+}O_9$ (M = Mg, Ca, Zn, Sr and Cd), $Ba_3M^{3+}Ir_2^{4.5+}O_9$ (M = Sc and In) and $Ba_3M^{4+}Ir_2^{4+}O_9$ (M = Ti and Zr). Magnetic susceptibility and specific heat measurements were carried out. In the $Ba_3M^{2+}Ir_2^{5+}O_9$, the Ir^{5+} ions have a non-magnetic ground state and the magnetic behavior for these compounds is explained by the Kotani's theory. For $Ba_3M^{4+}Ir_2^{4+}O_9$, the effective magnetic moment of these compounds is significantly small, although the Ir^{4+} ions have magnetic moment, which indicates the existence of the strong antiferromagnetic interaction between Ir^{4+} ions in the $Ir_2^{4+}O_9$ face-shared bioctahedra. In the case of $Ba_3M^{3+}Ir_2^{4.5+}O_9$, a specific heat anomaly was found at about 10 K (M = Sc) and 1.6 K (M = In), which suggests the magnetic ordering of the magnetic moments of Ir^{4+} in the $(Ir^{4+}Ir^{5+})O_9$ bioctahedra.

Keywords: 6H-perovskite; Iridium; Rietveld analysis; Magnetic susceptibility; Specific heat

1. Introduction

The perovskite oxides ABO_3 form a wide family of compounds, reflecting the flexibility in the chemical composition and crystal structure. Generally, their structures can be regarded as the stacking of close-packed AO_3 layers and the filling of subsequent octahedral sites by B-site ions. The difference in the stacking sequence changes the way of linkage of BO_6 octahedra: the corner-sharing BO_6 in the ideal cubic perovskite (3C: three-layer and cubic) with $abc\ldots$ sequence, the face-sharing BO_6 in 2H-perovskite (2H: two-layer and hexagonal) with $ab\ldots$ sequence, and mixed linkages between the corner- and face-sharing in various intergrowth structures [1].

It is known that the B-site ions normally determine the physical properties of the perovskite oxides ABO_3. Therefore, the perovskite-related oxides can show a variety of physical properties reflecting the nature of the B-site cations and the linkage of BO_6 octahedra. The oxides containing platinum-group metals at the B-site often exhibit interesting magnetic and electronic properties. For example, Sr_2RuO_4 is a superconductor with $T_c \sim 1$ K [2], Sr_2IrO_4 shows weak ferromagnetic behavior below 250 K [3] and $SrRuO_3$ is a metallic ferromagnet below 160 K [4].

Recently, the 6H-perovskites containing platinum-group metals, $Ba_3MM'_2O_9$ (M = alkali metals, alkaline earth elements, 3d transition metals, lanthanides; M' = Ru, Ir) [5–15] have been investigated. In those compounds, the stacking sequence of AO_3 layers is $abacbc\ldots$, and M and M' ions occupy the corner-sharing octahedral sites (MO_6) and the face-sharing octahedral ones (M'_2O_9 dimer), respectively. For many of these compounds, an antiferromagnetic spin-pairing occurs in the M'_2O_9 dimer even at room temperature. In the $Ba_3NaRu_2^{5.5+}O_9$ [10], the charge ordering between Ru^{5+} and Ru^{6+} ions (the formation of the $Ru_2^{5+}O_9$ and $Ru_2^{6+}O_9$ dimers) and the rapid decreasing of magnetic susceptibility were found below 210 K. In

*Corresponding author. Fax: +81 11 746 2557.
E-mail address: doi@sci.hokudai.ac.jp (Y. Doi).

0022-4596/$ - see front matter © 2006 Elsevier Inc. All rights reserved.
doi:10.1016/j.jssc.2006.04.055

addition, the $Ba_3MM'_2O_9$ compounds show the magnetic transitions at low temperatures, which originate from the magnetic interaction between M and M' ions.

In this paper, we focused our attention on compounds $Ba_3MIr_2O_9$ (M = Mg, Ca, Sc, Ti, Zn, Sr, Zr, Cd and In). They are expected to adopt various charge configurations of $Ba_3M^{2+}Ir_2^{5+}O_9$ (M = Mg, Ca, Zn, Sr and Cd), $Ba_3M^{3+}Ir_2^{4.5+}O_9$ (M = Sc and In) and $Ba_3M^{4+}Ir_2^{4+}O_9$ (M = Ti and Zr). All the M ions are non-magnetic in this case; thus, these compounds should show the characteristic magnetic behavior reflecting the different kinds of Ir_2O_9 dimers. We study systematically the crystallographic and magnetic properties of these compounds.

2. Experimental

2.1. Synthesis

Polycrystalline samples of compositions $Ba_3MIr_2O_9$ (M = Mg, Ca, Sc, Ti, Zn, Sr, Zr and In) were prepared by using standard solid-state techniques. As starting materials, $BaCO_3$, MgO, $CaCO_3$, Sc_2O_3, TiO_2, ZnO, $SrCO_3$, ZrO_2, In_2O_3 and Ir metal powders were used. They were weighed out in the appropriate metal ratios and well mixed in an agate mortar. The mixtures were pressed into pellets and then calcined at 900 °C for 12 h. Subsequently, the products were annealed at 1000–1300 °C for 12 h × 5–7 times with several interval regrindings and repelletings until a single $Ba_3MIr_2O_9$ phase was obtained. Final heating temperatures were 1100 °C (M = Ti, Zn, Sr), 1200 °C (Mg, Ca, Zr), and 1300 °C (Sc, In). For the preparation of $Ba_3CdIr_2O_9$, following starting materials were accurately weighed, i.e., BaO_2:CdO:IrO_2:Ir = 3:1:1:1, and were well mixed. The mixtures were ground and loaded in a platinum tube. The reaction was carried out in an evacuated quartz tube (to avoid the evaporation of CdO) at 1100 °C for 12 × 2 h with an interval grinding.

2.2. X-ray diffraction analysis

Powder X-ray diffraction patterns were collected with a Rigaku MultiFlex diffractometer using the monochromatic Cu-$K\alpha$ radiation in 2θ-steps of 0.02° and 7 s counting time in the range $10° \leqslant 2\theta \leqslant 120°$. The calculations were performed by the Rietveld method using the program RIETAN2000 [16]. The background and peak profiles were fitted by the Legendre polynomials and the split pseudo-Voigt function, respectively.

2.3. Magnetic susceptibility measurements

Magnetic susceptibility measurements were made in the temperature range of $1.8\,K \leqslant T \leqslant 400\,K$ using a SQUID magnetometer (Quantum Design, MPMS-5S). Data were collected under both zero-field-cooled (ZFC) and field-cooled (FC) conditions in an applied field of 0.5 T. For $Ba_3TiIr_2O_9$, the field dependence of the magnetization was measured at 5 K in the $-5\,T \leqslant H \leqslant 5\,T$.

2.4. Specific heat measurements

Specific heat measurements were performed using a relaxation technique by a commercial heat capacity measuring system (Quantum Design, PPMS model) in the temperature range of 1.8–300 K. In the case of $Ba_3InIr_2O_9$, the specific heat was measured in the temperature range of 0.55–300 K. The sintered sample in the form of a pellet was mounted on a thin alumina plate with grease for better thermal contact.

3. Results and discussion

3.1. Crystal structures

The title compounds were prepared as a single phase except for $Ba_3CdIr_2O_9$, which contains a small amount (~1%) of unknown impurity. The X-ray diffraction profiles for $Ba_3ZnIr_2O_9$ and $Ba_3SrIr_2O_9$ are shown in Figs. 1 (a) and (b), respectively. The diffraction data for M = Mg, Sc, Ti, Zn, Zr and In could be indexed with a hexagonal unit cell (a_h~5.8 Å, c_h~14 Å) and analyzed by the Rietveld method using a structural model for the 6H-perovskite $Ba_3LnIr_2O_9$ (space group $P6_3/mmc$) [17]. On the other hand, the data for M = Ca, Sr and Cd show many diffraction peaks indexed with a larger orthohexagonal cell ($a \sim a_h$, $b \sim \sqrt{3}a_h$, $c \sim c_h$). Finally, all the diffraction peaks were explained by a monoclinic cell with space group $C2/c$, and successfully refined by using a structural

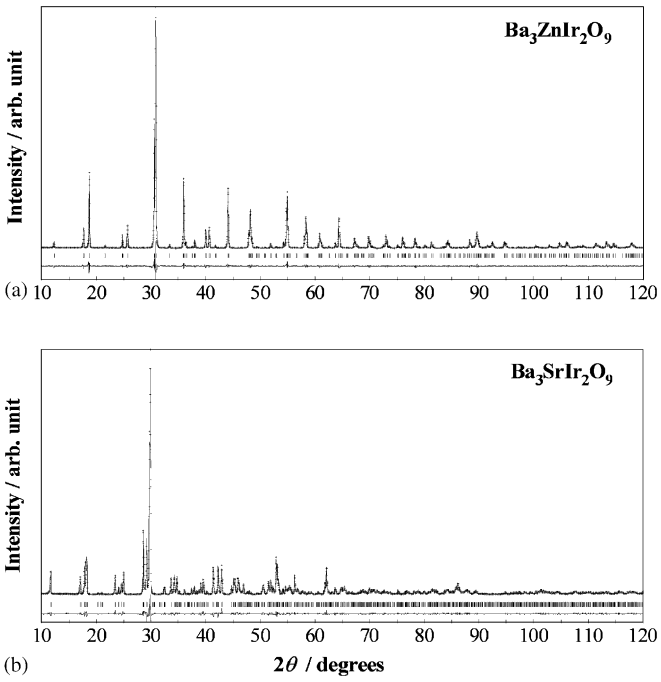

Fig. 1. X-ray diffraction profiles for (a) $Ba_3ZnIr_2O_9$ and (b) $Ba_3SrIr_2O_9$.

Table 1
Structural parameters for $Ba_3ZnIr_2O_9$ and $Ba_3SrIr_2O_9$

Atom	Site	x	y	z	B/Å^2
$Ba_3ZnIr_2O_9$					
Space group $P6_3/mmc$ (No. 194), $Z = 2$					
$a = 5.7833(1)$Å, $c = 14.3626(3)$Å					
$R_{wp} = 10.56\%$, $R_I = 1.44\%$, $R_e = 7.29\%$					
Ba(1)	2*b*	0	0	1/4	0.43(4)
Ba(2)	4*f*	1/3	2/3	0.9120(1)	0.46(3)
Zn	2*a*	0	0	0	0.10(7)
Ir	4*f*	1/3	2/3	0.1541(1)	0.20(2)
O(1)	6*h*	0.4810(7)	0.9620	1/4	0.76(10)
O(2)	12*k*	0.1687(6)	0.3374	0.4181(3)	0.76
$Ba_3SrIr_2O_9$					
Space group $C2/c$ (No. 15), $Z = 4$					
$a = 5.9988(1)$ Å, $b = 10.3305(3)$Å, $c = 15.1652(4)$Å, $\beta = 92.423(1)^\circ$					
$R_{wp} = 10.68\%$, $R_I = 1.87\%$, $R_e = 7.37\%$					
Ba(1)	4*e*	0	–0.0065(3)	1/4	0.78(7)
Ba(2)	8*f*	0.0119(3)	0.3335(3)	0.0980(1)	0.99(5)
Sr	4*a*	0	0	0	0.50(9)
Ir	8*f*	–0.0241(2)	0.3350(2)	0.8399(1)	0.28(3)
O(1)	4*e*	0	0.515(3)	1/4	1.4(2)
O(2)	8*f*	0.287(3)	0.236(1)	0.237(1)	1.4
O(3)	8*f*	0.044(2)	0.826(2)	0.097(1)	1.4
O(4)	8*f*	0.328(3)	0.088(2)	0.075(1)	1.4
O(5)	8*f*	0.786(2)	0.087(1)	0.111(1)	1.4

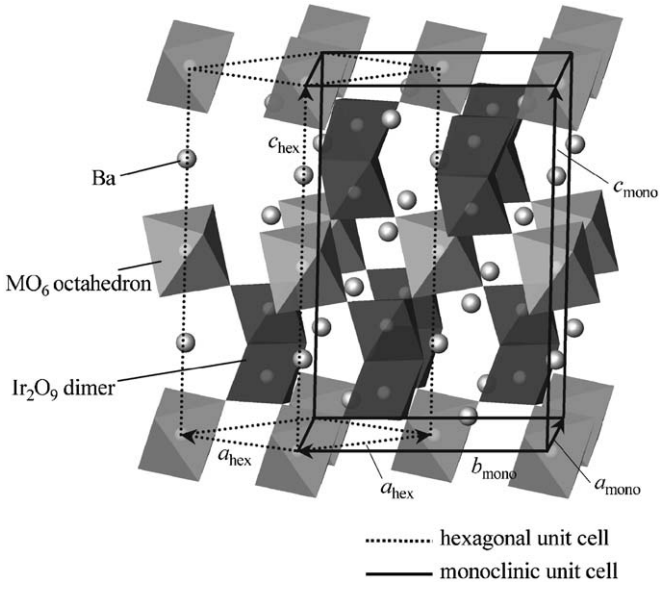

Fig. 2. The crystal structure of $Ba_3MIr_2O_9$ and a schematic illustration of the relationship of the unit cell between the hexagonal (dotted line) and monoclinic (solid line) cells.

model for $Ba_3SrRu_2O_9$ [18]. The structural parameters for $Ba_3ZnIr_2O_9$ (hexagonal) and $Ba_3SrIr_2O_9$ (monoclinic) are listed in Table 1. Those for the other compounds and the variation of lattice parameters with the six-coordinate ionic radius of M ions are shown in the Supplementary data. The schematic crystal structure of $Ba_3MIr_2O_9$ and a relationship between the hexagonal and monoclinic cells are shown in Fig. 2. In both structures, M and Ir ions occupy the six-coordinate sites, and two IrO_6 form an Ir_2O_9 dimer by face-sharing. Of these $Ba_3MIr_2O_9$ compounds, only $Ba_3ScIr_2O_9$ and $Ba_3TiIr_2O_9$ show a partial cation disordered arrangement between the M and Ir sites. The ratios of this disordered arrangement are 5.5(3) for $Ba_3ScIr_2O_9$ and 21.0(4) % for $Ba_3TiIr_2O_9$.

The variation of the Ir–Ir distance d(Ir–Ir) and the average Ir–O distance d(Ir–O) with the average oxidation state of Ir ion v(Ir) is plotted in Fig. 3. The Ir–Ir distance increases with the oxidation state of Ir; this is due to the electrostatic repulsion between Ir ions. The same tendency has been found in the Ru analog compounds $Ba_3MRu_2O_9$ [10]. However, the Ir–Ir distance of the $Ba_3Ti^{4+}Ir_2^{4+}O_9$ deviates from this tendency. This may be due to the above-mentioned cation disordered arrangement in the $Ba_3TiIr_2O_9$ compound. On the other hand, the average Ir–O distance decreases with increasing the oxidation state of Ir. This result reflects the change of the average valency of iridium ions in the $Ba_3MIr_2O_9$ compounds, i.e., it is Ir^{4+} (M = Ti and Zr), $Ir^{4.5+}$ (M = Sc and In) and Ir^{5+} (M = Mg, Ca, Zn, Sr and Cd).

The monoclinically distortion found in M = Ca, Sr and Cd compounds may be due to the mismatch in size between M and Ir ions. The ionic radii of M and Ir ions [19] for the $Ba_3MIr_2O_9$ compounds are listed in Table 2. Among compounds with the same valence condition, the monoclinically distortion is observed when the mismatch is too large. In addition, the partial disorder between the M and Ir sites is observed when it is relatively small. However, comparison among compounds with the different valence

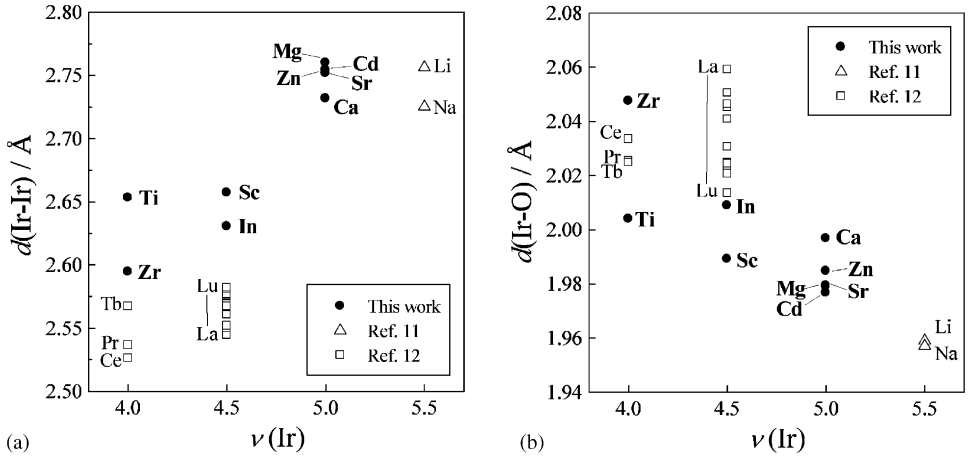

Fig. 3. (a) The variation of Ir–Ir distance d(Ir–Ir) against the average Ir valence v(Ir). (b) The variation of average Ir–O distance d(Ir–O) against the average Ir valence v(Ir). The data for other $Ba_3MIr_2O_9$ compounds are also plotted: M = Ce, Pr, Tb [12] for Ir^{4+}, M = Y, other lanthanide ions [12] for $Ir^{4.5+}$, and M = Li, Na [11] for $Ir^{5.5+}$. Note that there is a large standard deviation (~0.02 Å) of Ir–O lengths for the monoclinic phase (M = Ca, Sr, Cd).

Table 2
Ionic radii of M and Ir ions, and structural types for $Ba_3MIr_2O_9$ compounds

M	R_M [Å]	R_{Ir} [Å]	$\Delta = R_M - R_{Ir}$	Structure[a]	References
Li^+	0.76	—	—	H	[11]
Na^+	1.02	($Ir^{5.5+}$)	—	H	[11]
Mg^{2+}	0.72	0.570	0.150	H	This study
Zn^{2+}	0.74	(Ir^{5+})	0.170	H	This study
Cd^{2+}	0.95		0.380	M	This study
Ca^{2+}	1.00		0.430	M	This study
Sr^{2+}	1.18		0.610	M	This study
Sc^{3+}	0.745	0.598	0.147	H*	This study
In^{3+}	0.80	($Ir^{4.5+}$)	0.202	H	This study
Sm^{3+}–Lu^{3+}	0.958–0.861		0.36–0.263	H	[12]
Nd^{3+}	0.983		0.385	M	[12]
La^{3+}	1.032		0.434	M	[12]
Ti^{4+}	0.605	0.625	–0.02	H*	This study
Zr^{4+}	0.72	(Ir^{4+})	0.095	H	This study
Tb^{4+}	0.76		0.135	H	[12]
Pr^{4+}	0.85		0.225	H	[12]
Ce^{4+}	0.87		0.245	H	[12]

[a]H: hexagonal; M: monoclinic; *: partial disorder between M and Ir sites.

condition is not simple, because the difference in the strength of Ir–Ir repulsion may also affect the structure.

3.2. Magnetic properties and specific heat

3.2.1. $Ba_3M^{2+}Ir_2^{5+}O_9$ (M = Mg, Ca, Zn and Sr)

Fig. 4 shows the temperature dependence of the magnetic susceptibility for $Ba_3MgIr_2O_9$. All the $Ba_3M^{2+}Ir_2^{5+}O_9$ compounds are paramagnetic in the temperature range of 1.8–400 K. The electronic configuration of Ir^{5+} is $[Xe]4f^{14}5d^4$. It is known that in a strong octahedral field, the pentavalent iridium ion has a low spin configuration ($t_{2g}^4e_g^0$). In this case, the unquenched orbital angular momentum affects the magnetic properties. According to the Kotani's theory [20], the effective

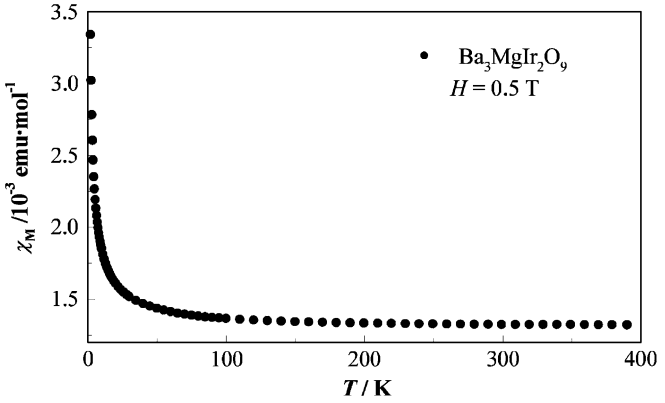

Fig. 4. The temperature dependence of the magnetic susceptibility for $Ba_3MgIr_2O_9$.

magnetic moment for low spin configuration of Ir^{5+}, μ_{eff} (Ir^{5+}), depends on the spin–orbit coupling constant and temperature:

$$\mu_{eff}^2(Ir^{5+}) \approx \frac{72k_BT}{\xi}, \quad (1)$$

where ξ is the spin–orbit coupling constant for Ir^{5+} and k_B is the Boltzmann constant. When $k_BT \ll \xi$, μ_{eff}^2 (Ir^{5+}) is approximately proportional to temperature T.

Fig. 5 shows the temperature dependence of $\mu_{eff}^2 = 3k_B\chi_M T/2N_A\mu_B^2$ for $Ba_3MIr_2O_9$ (M = Mg, Ca, Zn and Sr). The μ_{eff}^2 for these compounds increase linearly with temperature T. The spin–orbit coupling constant for the Ir^{5+} ion was calculated from the Eq. (1) and listed in Table 3. They are about 9000 cm^{-1}. These results are in agreement with the data reported previously, e.g. 8900 cm^{-1} (Sr_2ScIrO_6) and 8850 cm^{-1} (Ba_2YIrO_6) [21].

3.2.2. $Ba_3M^{4+}Ir_2^{4+}O_9$ (M = Ti and Zr)

The temperature dependence of the magnetic susceptibility for $Ba_3TiIr_2O_9$ and $Ba_3ZrIr_2O_9$ is plotted in Fig. 6(a). The magnetic susceptibility for $Ba_3TiIr_2O_9$ shows a divergence between the ZFC and FC susceptibilities below ~60 K. On the other hand, $Ba_3ZrIr_2O_9$ is paramagnetic down to 1.8 K and no divergence between the ZFC and FC susceptibilities is observed. In order to estimate the effective magnetic moment of Ir^{4+} ion in these two compounds, the susceptibility data were fitted using a modified Curie–Weiss law:

$$\chi_M = \frac{C}{T-\theta} + \chi_{TIP}. \quad (2)$$

The effective magnetic moment obtained from the Curie constant (C), Weiss constant (θ) and temperature-independent paramagnetic susceptibility (χ_{TIP}) are 0.26(1) μ_B/Ir, 34 (4) K and $5.4(1)\times10^{-4}$ emu mol^{-1} respectively, for $Ba_3TiIr_2O_9$, and 0.28(1) μ_B/Ir, 21(3) K and $4.4(1)\times10^{-4}$ emu mol^{-1}, respectively, for $Ba_3ZrIr_2O_9$.

Different from the case for the Ir^{5+} ion, an Ir^{4+} ion has odd d-electrons ($5d^5$); therefore the Ir^{4+} ion must have a magnetic moment. However, the effective magnetic moments of these two compounds are rather smaller compared with that expected for two free Ir^{4+} ions (1.73 μ_B/Ir for the low spin state). This result suggests that an antiferromagnetic spin-paring of Ir^{4+} ions occurs in the $Ir_2^{4+}O_9$ dimer, which is the same result as $Ba_3Ce^{4+}Ir_2^{4+}O_9$ [12].

The temperature dependence of the specific heat for $Ba_3TiIr_2O_9$ is plotted in Fig. 6(b). No anomaly was observed even at 60 K, at which the divergence between the ZFC and FC susceptibility was found. This result indicates that the long-range magnetic ordering of Ir^{4+} does not occur between 1.8 and 300 K. The magnetization measurement was carried out at 5 K, and showed the existence of the small hysteresis loop

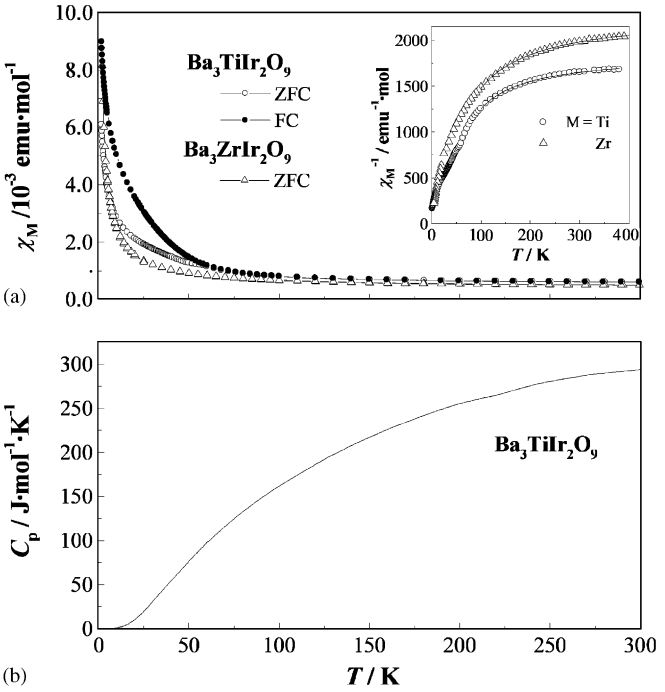

Fig. 6. The temperature dependence of (a) the magnetic susceptibility for $Ba_3TiIr_2O_9$ and $Ba_3ZrIr_2O_9$, and (b) the specific heat for $Ba_3TiIr_2O_9$. In (a), the inset shows the reciprocal magnetic susceptibility and the Curie–Weiss fitting (solid curve).

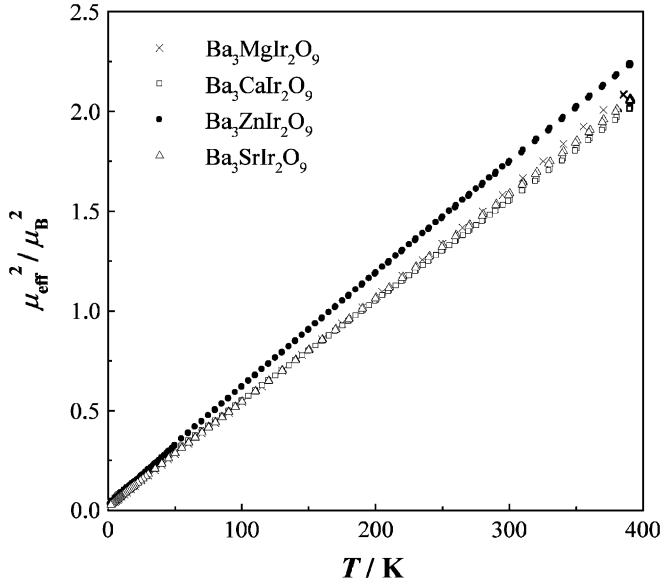

Fig. 5. The temperature dependence of μ_{eff}^2 for $Ba_3M^{2+}Ir_2^{5+}O_9$.

Table 3
Spin–orbit coupling constants for $Ba_3MIr_2O_9$ (M = Mg, Ca, Zn and Sr)

Compounds	ξ (cm^{-1})
$Ba_3MgIr_2O_9$	9615(4)
$Ba_3CaIr_2O_9$	8746(8)
$Ba_3ZnIr_2O_9$	9935(6)
$Ba_3SrIr_2O_9$	8771(1)

with the residual magnetization of $\sim 0.0002\,\mu_B$/Ir. The susceptibility anomaly at 60 K may be due to a small amount of unknown impurity or the short-range ordering of unpaired Ir^{4+} moments derived from the partial disorder arrangement.

3.2.3. $Ba_3M^{3+}Ir_2^{4.5+}O_9$ (M = Sc and In)

Fig. 7(a) shows the temperature dependence of the magnetic susceptibility for $Ba_3ScIr_2O_9$ and $Ba_3InIr_2O_9$. The susceptibility data in the high temperature region ($T > 200$ K) are fitted using the modified Curie–Weiss law (Eq. (2)). The effective magnetic moment, Weiss constant and temperature-independent paramagnetic susceptibility for $Ba_3ScIr_2O_9$ are 1.27(8) μ_B/Ir (1.79 μ_B/formula unit), $-570(52)$ K and $6.3(3)\times10^{-4}$ emu mol^{-1}, respectively, and for $Ba_3InIr_2O_9$ are 1.08(6) μ_B/Ir (1.53 μ_B/formula unit), $-310(30)$ K and $7.5(3)\times10^{-4}$ emu mol^{-1}, respectively. These effective magnetic moments are rather higher than that of $Ba_3M^{4+}Ir_2^{4+}O_9$ compounds in this study, and close to the magnetic moment for $S=\frac{1}{2}$ ion. When the Ir^{5+} ion is in a singlet ground state and that the Ir^{4+} ion has a magnetic moment of $S=\frac{1}{2}$ (i.e., it is in the low spin state), this result indicates that there exist both the Ir^{4+} and Ir^{5+} ions in the Ir_2O_9 dimer.

The temperature dependence of the specific heat divided by temperature (C_p/T) for $Ba_3ScIr_2O_9$ and $Ba_3InIr_2O_9$ is plotted in Figs. 8(a) and (b), respectively. The specific heat anomaly observed at about 10 K for $Ba_3ScIr_2O_9$ corresponds to the anomaly in its $d\chi_M/dT$ vs., T curve (Fig. 7(b)). For $Ba_3InIr_2O_9$, no anomaly is observed in the magnetic susceptibility measurements down to 1.8 K, and its specific heat measurements show an anomaly at 1.6 K. In order to estimate the magnetic entropy change (ΔS_m) due to the magnetic ordering, the magnetic entropy (S_m) was calculated by $S_m = \int C_m/T\,dT$. The magnetic specific heat C_m was obtained by subtracting the contribution of lattice specific heat from the observed specific heat. This contribution was estimated by using a polynomial function of the temperature, $f(T) = aT^3 + bT^5 + cT^7$ [22]. These constants (a, b and c) were determined by fitting this function to the observed specific heat data between 20 and 30 K. The temperature dependence of the magnetic entropy for $Ba_3ScIr_2O_9$ and $Ba_3InIr_2O_9$ is shown in Fig. 8. The magnetic entropy changes ΔS_m were determined to be 1.9 J mol^{-1} K^{-1} for $Ba_3ScIr_2O_9$ and 3.7 J mol^{-1} K^{-1} for $Ba_3InIr_2O_9$. These values are comparable to $R\ln(2S+1) = R\ln 2 = 5.76$ J mol^{-1} K^{-1} ($S=1/2$); thus, these anomalies may be due to the magnetic ordering (possibly, antiferromagnetic one) of Ir^{4+} moments in $Ir_2^{4.5+}O_9$ dimers. Although observed ΔS_m are smaller than $R\ln 2$, the similar values were also found in analogous compounds $Ba_3Y^{3+}Ir_2^{4.5+}O_9$ and $Ba_3Lu^{3+}Ir_2^{4.5+}O_9$ ($\Delta S_m \sim 3.6$ J mol^{-1} K^{-1}) [12]. Further the reduction in the ΔS_m of $Ba_3ScIr_2O_9$ may be caused by the cation-disordered arrangement between Sc and Ir ions.

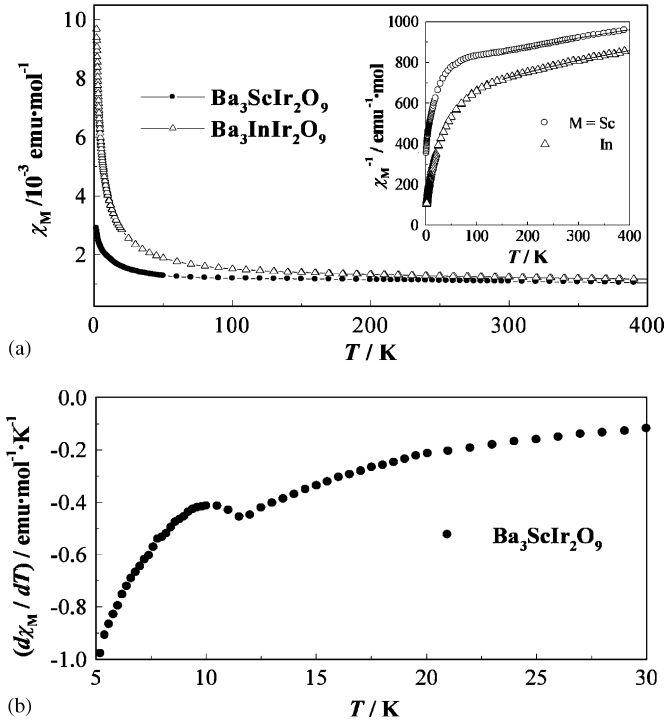

Fig. 7. (a) The temperature dependence of the magnetic susceptibility for $Ba_3ScIr_2O_9$ and $Ba_3InIr_2O_9$. The inset shows the reciprocal magnetic susceptibility and the Curie–Weiss fitting. (b) The first derivative of the magnetic susceptibility of $Ba_3ScIr_2O_9$ ($d\chi_M$/dT) in the temperature range of 5–30 K.

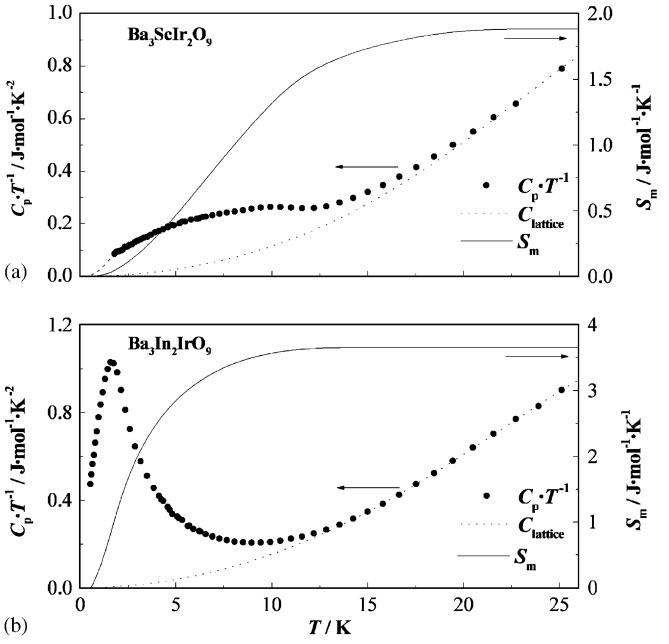

Fig. 8. The temperature dependence of the specific heat and the magnetic entropy for (a) $Ba_3ScIr_2O_9$ and (b) $Ba_3InIr_2O_9$. In (a), the specific heat data below 1.8 K were extrapolated from the curve of $C_p/T \propto T^2$ (a dashed line). The contribution of the lattice specific heat was estimated by using a polynomial function of the temperature $f(T) = aT^3 + bT^5 + cT^7$ (see text).

4. Summary

Crystal structures and magnetic properties of 6H-perovskite-type oxides $Ba_3MIr_2O_9$ (M = non-magnetic ions: Mg^{2+}, Ca^{2+}, Sc^{3+}, Ti^{4+}, Zn^{2+}, Sr^{2+}, Zr^{4+}, Cd^{2+} and In^{3+}) have been investigated. Many of these compounds adopt the hexagonal structure, while the compounds with the larger difference in size between M and Ir ions (M = Ca, Sr, Cd) adopt the monoclinically distorted structure. Among compounds with the same valence condition, the smaller difference in size brings about the partial disorder between the M and Ir sites (M = Sc and Ti).

The magnetic behavior of $Ba_3MIr_2O_9$ can be regarded as that of the Ir_2O_9 dimer. The $Ir_2^{5+}O_9$ and $Ir_2^{4+}O_9$ dimers show no magnetic transition in the experimental temperature range (1.8–400 K). On the other hand, the magnetic transition was observed for the compounds with $Ir_2^{4.5+}O_9$ dimer (M = Sc and In), which may be due to the antiferromagnetic magnetic ordering of unpaired Ir^{4+} ions.

Appendix A. Supplementary data

Supplementary data associated with this article can be found in the online version at doi:10.1016/j.jssc.2006.04.055.

References

[1] J.M. Longo, J.A. Kafalas, J. Solid State Chem. 1 (1969) 103–108.
[2] Y. Maeno, H. Hashimoto, K. Yoshida, S. Nishizaki, T. Fujita, J.G. Bednorz, F. Lichtenberg, Nature 372 (1994) 532–534.
[3] M.K. Crawford, M.A. Subramanian, R.L. Harlow, J.A. Fernandez-baca, Z.R. Wang, D.C. Johnston, Phys. Rev. B 49 (1994) 9198–9201.
[4] A. Callaghan, C.W. Moeller, R. Ward, Inorg. Chem. 5 (1966) 1572–1576.
[5] P. Lightfoot, P.D. Battle, J. Solid State Chem. 89 (1990) 174–183.
[6] J.T. Rijssenbeek, Q. Huang, R.W. Erwin, H.W. Zandbergen, R.J. Cava, J. Solid State Chem. 146 (1999) 65–72.
[7] Y. Doi, Y. Hinatsu, Y. Shimojo, Y. Ishii, J. Solid State Chem. 161 (2001) 113–120.
[8] Y. Doi, M. Wakeshima, Y. Hinatsu, A. Tobo, K. Ohoyama, Y. Yamaguchi, J. Mater. Chem. 11 (2001) 3135–3140.
[9] Y. Doi, K. Matsuhira, Y. Hinatsu, J. Solid State Chem. 165 (2002) 317–323.
[10] K.E. Stitzer, M.D. Smith, W.R. Gemmill, H.-C. zur Loye, J. Am. Chem. Soc. 124 (2002) 13877–13885.
[11] S.-J. Kim, M.D. Smith, J. Darriet, H.-C. zur Loye, J. Solid State Chem. 177 (2004) 1493–1500.
[12] Y. Doi, Y. Hinatsu, J. Phys.: Condens. Matter 16 (2004) 2849–2860.
[13] Y. Doi, Y. Hinatsu, J. Solid State Chem. 177 (2004) 3239–3244.
[14] M.W. Lufaso, H.-C. zur Loye, Inorg. Chem. 44 (2005) 9143–9153.
[15] M.W. Lufaso, H.-C. zur Loye, Inorg. Chem. 44 (2005) 9154–9161.
[16] F. Izumi, T. Ikeda, Mater. Sci. Forum 321-324 (2000) 198–203.
[17] I. Thumm, U. Treiber, S. Kemmler-Sack, J. Solid State Chem. 35 (1980) 156–166.
[18] J. Darriet, M. Drillon, G. Villeneuve, P. Hagenmuller, J. Solid State Chem. 19 (1976) 213–220.
[19] R.D. Shannon, Acta Crystallogr. A 32 (1976) 751–767.
[20] M. Kotani, J. Phys. Soc. Japan 4 (1949) 293–297.
[21] M. Wakeshima, D. Harada, Y. Hinatsu, J. Alloys Compd. 287 (1999) 130–136.
[22] J.E. Gordon, R.A. Fisher, Y.X. Jia, N.E. Phillips, S.F. Reklis, D.A. Wright, A. Zettl, Phys. Rev. B 59 (1999) 127–130.